

Fine and hyperfine splitting of the low-lying states of ${}^9\text{Be}$

Mariusz Puchalski,¹ Jacek Komasa,¹ and Krzysztof Pachucki²

¹Faculty of Chemistry, Adam Mickiewicz University, Uniwersytetu Poznańskiego 8, 61-614 Poznań, Poland

²Faculty of Physics, University of Warsaw, Pasteura 5, 02-093 Warsaw, Poland

(Dated: May 3, 2022)

We perform accurate calculations of energy levels as well as fine and hyperfine splittings of the lowest ${}^1,{}^3P_J$, 3S_1 , ${}^3P_J^e$, and ${}^1,{}^3D_J$ excited states of the ${}^9\text{Be}$ atom using explicitly correlated Gaussian functions and report on the breakdown of the standard hyperfine structure theory. Because of the strong hyperfine mixing, which prevents the use of common hyperfine constants, we formulate a description of the fine and hyperfine structure that is valid for an arbitrary coupling strength and may have wide applications in many other atomic systems.

PACS numbers: 31.15.ac, 31.30.J-

I. INTRODUCTION

The main drawback of atomic structure methods based on the wave function represented as a linear combination of determinants of spin-orbitals (Hartree-Fock, configuration interaction, multi-configurational self-consistent field, etc.) is the difficulty in providing results with reliably estimated uncertainties. While the accuracy of nonrelativistic energy can be assessed by increasing the space of electronic configurations, the irregular convergence of matrix elements, especially involving singular operators, such as those for relativistic or quantum electrodynamics (QED) corrections, often does not allow for presenting any uncertainties. Therefore, this deficiency limits the use of these methods in the high-accuracy-demanding applications, e.g. testing quantum electrodynamics [1–3], determination of the nuclear charge radii [4–7], the nuclear electromagnetic moments [8, 9], or physical constants [10], and searching for new physics [11]. It is desirable therefore to develop tools which provide high and controlled accuracy, like those based on explicitly correlated basis functions, e.g. exponential, Hylleraas, or Gaussian (ECG) ones. The controlled accuracy is achieved by means of a full variational optimization of the wave function and by transformation of singular operators to an equivalent but more regular form. The price paid for using the explicitly correlated functions is the rapid increase in the complexity of calculations with each additional electron; therefore, application of these functions has so far been limited to few-electron systems only.

Before passing to the main topic, which is the 4-electron beryllium (Be) atom, let us briefly describe recent advances in the calculation of 1-, 2-, and 3-electron atomic systems. Hydrogenic systems are the only ones in which theoretical predictions including QED effects are sufficiently accurate to determine the nuclear (proton, deuteron) charge radius from the measured transition frequencies [10]. Being apparently simple, hydrogenic systems are a cornerstone for the implementation of QED in bound states, which relies on the expansion of binding energy in powers of the fine structure constant $\alpha \sim 1/137$. Similarly, for two- and more-electron systems, one also performs expansion in α , as long as the nuclear charge Z is not too large. This allows description of an atomic system in terms of the successively smaller effects, i.e. nonrelativistic energy α^2 , relativistic correction α^4 , lead-

ing QED of order α^5 , and so on. For the helium atom all these expansion terms are calculated up to the order α^6 [12], with some states up to the order α^7 [13]. Such high order calculations are feasible with explicitly correlated exponential basis functions, for which analytic integrals are known. Atomic systems with three electrons present greater difficulty for the accurate calculation of their energy levels despite obtaining very precise wave functions with explicitly correlated Hylleraas or ECG functions. Nevertheless, several highly accurate results have been obtained for Li and Be^+ , including isotope shifts for the charge radii determination [4, 14, 15], and fine [16] and hyperfine [17] splitting. The fine structure splitting of the lithium 2P_J state with the inclusion of $O(\alpha^6)$ QED corrections [16, 18] agrees well with even more accurate experimental values [19, 20], while current theoretical predictions for the ${}^6/{}^7\text{Li}$ ground state hyperfine splitting are limited by insufficient knowledge of the nuclear structure, and not by the atomic structure theory.

The experience gained from the above-mentioned systems can be exploited to a large extent in four-electron systems, but these ones are much more demanding in calculations. The attempts employing Hylleraas wave functions [21–23] are limited to nonrelativistic energy because of the lack of effective methods of evaluation of "relativistic" four-electron integrals. Therefore, our choice is the use of the ECG method, which performs very well for both nonrelativistic and relativistic contributions [21–43]. Nonetheless, we note that because Gaussian-type wave functions do not satisfy the Kato cusp condition, the complete calculation of the α^6 correction is still unfeasible. This unsolved problem limits the current capabilities of the ECG method in the application to three- and more-electron systems. After all, the ECG functions are so far the best suited for the four-electron systems and such an application to the Be atom will be presented here.

In our previous works on Be we have obtained accurate energies for the ground $2s^2 {}^1S_0$ and the excited $2s2p {}^1P_1$ states [39], the difference of which at $42\,565.441(11)\text{ cm}^{-1}$, agrees well with the experimental value of $42\,565.4501(13)\text{ cm}^{-1}$ obtained by Cook *et al.* [44] and with later calculations [45]. Last year, two more transitions were measured to a high accuracy—the wavenumber of the $2s^2 {}^1S_0 - 2s3d {}^1D_2$ line, equal to $64\,428.403\,21(55)\text{ cm}^{-1}$, and of the $2s2p {}^1P_1 - 2s3d {}^1D_2$ line, equal to $21\,862.952\,9(14)\text{ cm}^{-1}$, were reported

by Cook *et al.* [46]. In this case, no theoretical results at an adequate level of accuracy have been calculated yet. Moreover, in the beryllium atom, of particular theoretical interest is the lowest $2s2p\,{}^3P$ excited state, because it is metastable. So far though, its energy has not been measured and calculated to such a high accuracy as for the $2s2p\,{}^1P$ state. An old but the most accurate experimental excitation energy from the ground to the $2s2p\,{}^3P_1$ level equal to $21\,978.92(1)\text{ cm}^{-1}$ [47] is in agreement with the less accurate recent theoretical value of $21\,978.2(11)\text{ cm}^{-1}$ by Kedziora *et al.* [43]. Quite recently, the hyperfine splitting of the $2s2p\,{}^3P$ state has been accurately calculated and, with the help of the 50-years old measurements by Blachman [48], has been employed to determine the most accurate value of the electric quadrupole moment of ${}^9\text{Be}$ [9], but it is in disagreement with all previous determinations. Moreover, all the other Be energy levels lying below the ionization threshold of $75\,192.64\text{ cm}^{-1}$ have large uncertainties, being in the range $0.01 - 0.2\text{ cm}^{-1}$ [49], and there are no corresponding accurate theoretical results to compare with.

The purpose of the present work is therefore to significantly advance the theoretical description of the lowest excited states with different internal symmetries. Namely, we focus on states with non-vanishing spin or orbital angular momentum and verify the previous literature results, which were obtained using either the ECG method or methods based on one-electron approximation. More precisely, we report on ECG calculations for the six lowest excited states of the ${}^9\text{Be}$ atom: ${}^1,{}^3P_J$, 3S_1 , ${}^3P_J^e$, and ${}^1,{}^3D_J$, including their fine and hyperfine splittings. Due to a significant hyperfine mixing, the standard hyperfine structure formulation in terms of A_J and B_J coefficients is not adequate in some cases. For this reason we have introduced a combined fine–hyperfine structure formalism that naturally accounts for an arbitrary mixing between fine and hyperfine levels. Moreover, in order to unify the description of atomic wave functions of different symmetries, we have introduced in this work a Cartesian angular momentum representation, which is tailored for use with many-electron explicitly correlated basis functions and which simplifies evaluation of matrix elements.

II. THEORETICAL FRAMEWORK

In the calculations of the energy levels of few-electron light atomic systems, we employ the expansion in the fine-structure constant $\alpha \approx 1/137$

$$E(\alpha) = E^{(2)} + E^{(4)} + E^{(5)} + E^{(6)} + \dots \text{ with } E^{(n)} \sim m\alpha^n, \quad (1)$$

and some expansion terms may include finite powers of $\ln \alpha$

A. Nonrelativistic energy

The leading term $E_0 \equiv E^{(2)}$ is obtained from the non-relativistic Hamiltonian in the center-of-mass system ($\vec{p}_N = -\sum_a \vec{p}_a$) by solving the Schrödinger equation (in natural

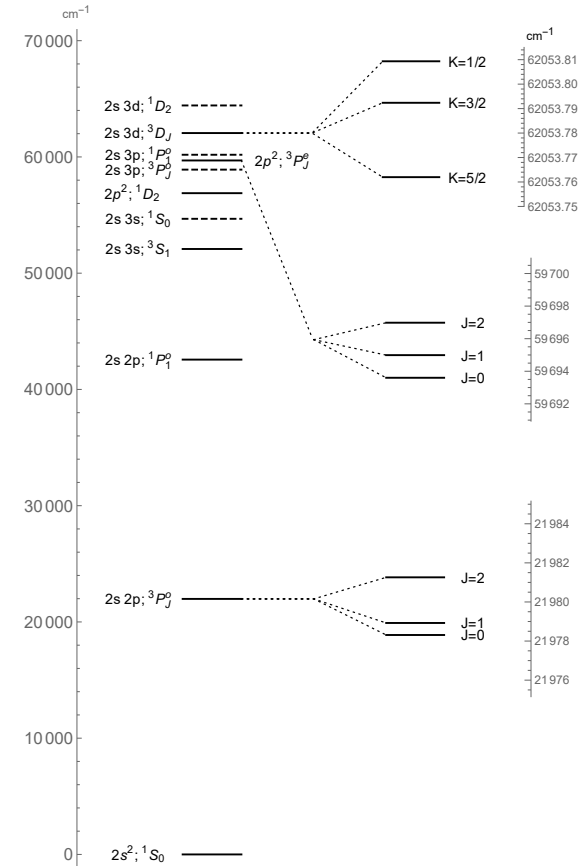


FIG. 1. The lowest energy levels of the Be atom. The levels for which the energy is evaluated in this work are drawn in solid lines and the remaining ones in dashed line. The fine structure of the triplet states of our interest is also shown, $\vec{J} = \vec{L} + \vec{S}$, $\vec{K} = \vec{I} + \vec{S}$.

units)

$$H^{(2)}\Psi = E_0\Psi \quad (2)$$

$$H^{(2)} = \frac{\vec{p}_N^2}{2m_N} + \sum_a \frac{\vec{p}_a^2}{2m} - \sum_a \frac{Z\alpha}{r_a} + \sum_{a < b} \frac{\alpha}{r_{ab}} \quad (3)$$

where Z is the nuclear charge, and m and m_N are the electron and nuclear masses, respectively. In this work, the effects of the finite nuclear mass (recoil) are included in $H^{(2)}$. This is in contrast to the perturbative approach based on additional expansion in the electron-nucleus mass ratio, which is particularly useful in the isotope shift calculations [40]. Once the wave function Ψ is determined, all the corrections to the non-relativistic energy E_0 can be expressed in terms of expectation values $\langle \Psi | \dots | \Psi \rangle \equiv \langle \dots \rangle$ of known operators.

B. Leading order corrections

The leading relativistic $E^{(4)}$ correction is calculated as the mean value of the Breit-Pauli Hamiltonian [50]. For convenience, we split this Hamiltonian, according to its inner composition, into three parts: the no-spin (ns), the fine-structure

(fs), and the hyperfine-structure (hfs) part

$$H^{(4)} = H_{\text{ns}}^{(4)} + H_{\text{fs}}^{(4)} + H_{\text{hfs}}^{(4)}. \quad (4)$$

The spin-independent part in its explicit form is

$$\begin{aligned} H_{\text{ns}}^{(4)} = & \sum_a \left[-\frac{\vec{p}_a^4}{8m^3} + \frac{\pi Z \alpha}{2m^2} \delta^3(r_a) \right. \\ & + \frac{Z \alpha}{2m m_N} p_a^i \left(\frac{\delta^{ij}}{r_a} + \frac{r_a^i r_a^j}{r_a^3} \right) p_N^j \Big] \\ & + \sum_{a < b} \left[\frac{\pi \alpha}{m^2} \delta^3(r_{ab}) - \frac{\alpha}{2m^2} p_a^i \left(\frac{\delta^{ij}}{r_{ab}} + \frac{r_{ab}^i r_{ab}^j}{r_{ab}^3} \right) p_b^j \right]. \end{aligned} \quad (5)$$

The part related to the fine-structure effects, containing the vector $\vec{\sigma}_a$ of Pauli spin matrices of electron a , can be expressed as follows

$$\begin{aligned} H_{\text{fs}}^{(4)} = & \sum_a \frac{Z \alpha}{4} \vec{\sigma}_a \cdot \left[\frac{(g-1)}{m^2} \frac{\vec{r}_a}{r_a^3} \times \vec{p}_a - \frac{g}{m m_N} \frac{\vec{r}_a}{r_a^3} \times \vec{p}_N \right] \\ & + \sum_{a \neq b} \frac{\alpha}{4m^2} \vec{\sigma}_a \cdot \left[g \frac{\vec{r}_{ab}}{r_{ab}^3} \times \vec{p}_b - (g-1) \frac{\vec{r}_{ab}}{r_{ab}^3} \times \vec{p}_a \right] \\ & - \sum_{a < b} \frac{3\alpha g^2}{16m^2} \sigma_a^i \sigma_b^j \left(\frac{r_{ab}^i r_{ab}^j}{r_{ab}^5} - \frac{\delta^{ij}}{3r_{ab}^3} \right), \end{aligned} \quad (6)$$

where g is the free electron g -factor, which accounts for one-loop QED corrections. Finally, the leading order Hamiltonian for the hyperfine splitting, containing the nuclear spin \vec{I} , reads

$$\begin{aligned} H_{\text{hfs}}^{(4)} = & \sum_a \left[\frac{1}{3} \frac{Z \alpha g g_N}{m m_N} \vec{\sigma}_a \cdot \vec{I} \pi \delta^3(r_a) \right. \\ & + \frac{Z \alpha g_N}{2m m_N} \vec{I} \cdot \frac{\vec{r}_a}{r_a^3} \times \vec{p}_a - \frac{Z \alpha (g_N - 1)}{2m_N^2} \vec{I} \cdot \frac{\vec{r}_a}{r_a^3} \times \vec{p}_N \\ & + \frac{3Z \alpha g g_N}{8m m_N} \sigma_a^i I^j \left(\frac{r_a^i r_a^j}{r_a^5} - \frac{1}{3} \frac{\delta^{ij}}{r_a^3} \right) \\ & \left. - \frac{\alpha Q_N}{2} \left(\frac{r_a^i r_a^j}{r_a^5} - \frac{1}{3} \frac{\delta^{ij}}{r_a^3} \right) \frac{3I^i I^j}{I(2I-1)} \right]. \end{aligned} \quad (7)$$

Here, Q_N is the electric quadrupole moment of the nucleus, and g_N is the nuclear g -factor defined by

$$g_N = \frac{m_N}{Z m_p} \frac{\mu}{\mu_N} \frac{1}{I}. \quad (8)$$

C. Higher order corrections

1. Centroid energy

Higher-order corrections, $E^{(n)}$ with $n > 4$, are usually much smaller than $E^{(4)}$ because they contain higher powers of α . The explicit form of the $m\alpha^5$ terms is given by

$$E^{(5)} = \frac{4Z\alpha^2}{3m^2} \left[\frac{19}{30} + \ln(\alpha^{-2}) - \ln k_0 \right] \sum_a \langle \delta^3(r_a) \rangle$$

$$+ \frac{\alpha^2}{m^2} \left[\frac{164}{15} + \frac{14}{3} \ln \alpha \right] \sum_{a < b} \langle \delta^3(r_{ab}) \rangle \quad (9)$$

$$- \frac{7}{6\pi} m \alpha^5 \sum_{a < b} \left\langle P \left(\frac{1}{m \alpha r_{ab}^3} \right) \right\rangle, \quad (10)$$

where $\ln k_0$ is the Bethe logarithm [50, 51], and $P(1/r^3)$ is the Araki-Sucher term [52, 53].

A complete set of operators for the quantum electrodynamic $m\alpha^6$ correction to energy levels of light atoms has been derived recently [54]. However, due to the lack of a computational method suitable for a four-electron wave function, we use the following approximate formula related to the hydrogenic Lamb shift

$$E^{(6)} \approx \frac{\pi Z^2 \alpha^3}{m^2} \left[\frac{427}{96} - 2 \ln(2) \right] \sum_a \langle \delta^3(r_a) \rangle \quad (11)$$

and estimate its uncertainty to be about 25%.

2. Fermi contact interaction

The hyperfine Hamiltonian in Eq. (7) represents the leading hyperfine interactions, but there are also other small corrections which contain higher powers of the fine structure constant α . Because most of them are proportional to the Fermi contact interaction, we account for them in terms of the $1 + \epsilon$ factor multiplying the first term of the $H_{\text{fs}}^{(4)}$ Hamiltonian

$$(1 + \epsilon) \frac{1}{3} \frac{Z \alpha g g_N}{m m_N} \sum_a \vec{\sigma}_a \cdot \vec{I} \pi \delta^3(r_a). \quad (12)$$

Below, we briefly describe contributions included in the ϵ factor.

The $\mathcal{O}(\alpha)$ correction is analogous to that in hydrogenic systems [55] and is due to the finite nuclear size and the nuclear polarizability. It is given by [55, 56]

$$H_Z^{(5)} = \left[-2Z\alpha m r_Z \right] \vec{I} \cdot \sum_a \frac{2}{3} \frac{Z \alpha g_N}{m m_N} \vec{\sigma}_a \pi \delta^3(r_a), \quad (13)$$

where r_Z is a kind of effective nuclear radius called the Zemach radius. Disregarding the inelastic effects, this radius can be written in terms of the electric charge ρ_E and magnetic-moment ρ_M densities as

$$r_Z = \int d^3r d^3r' \rho_E(r) \rho_M(r') |\vec{r} - \vec{r}'|. \quad (14)$$

Nevertheless, the inelastic, i.e. polarizability, corrections can be significant, but because they are very difficult to calculate, they are usually neglected. In this work we account for possible inelastic effects by employing $r_Z = 4.07(5)$ fm achieved from a comparison of very accurate calculations of hfs in ${}^9\text{Be}^+$ with the experimental value [56]. Because this correction is also proportional to the contact Fermi interaction, we represent it in terms of $\epsilon_Z = -0.000\,615$. There is a small recoil correction at the same order of α , for which we refer to [9, 57] and it contributes $\epsilon_{\text{rec}} = -0.000\,011$.

Next, there are radiative and relativistic corrections of the relative order $\mathcal{O}(\alpha^2)$. The radiative correction, beyond that included by the free electron g -factor, is [55]

$$H_{\text{rad}}^{(6)} = Z \alpha^2 \left(\ln 2 - \frac{5}{2} \right) \vec{I} \cdot \sum_a \frac{2}{3} \frac{Z \alpha g_N}{m m_N} \vec{\sigma}_a \pi \delta^3(r_a) \quad (15)$$

and the corresponding ϵ factor is $\epsilon_{\text{rad}} = -0.000384$. The $\mathcal{O}(\alpha^2)$ relativistic and higher order corrections are much more complicated. They have been calculated for the ground state of ${}^9\text{Be}^+$ [56]. Here we take this result and assume that it is proportional to the Fermi contact interaction, and obtain $\epsilon_{\text{rel}} = 0.001664$. The resulting total ϵ -correction is

$$\epsilon = \epsilon_Z + \epsilon_{\text{rec}} + \epsilon_{\text{rad}} + \epsilon_{\text{rel}} = 0.654 \cdot 10^{-3}. \quad (16)$$

Some previous works present these multiplicative corrections for all individual hyperfine contributions, but in our opinion this cannot be fully correct because higher order relativistic corrections may include additional terms, beyond that in H_{eff} in Eq. (57). These corrections are expected to be smaller than the experimental uncertainty and therefore are neglected here.

III. WAVE FUNCTION

In this section, we introduce the angular momentum formalism appropriate for explicitly correlated multielectron wave functions, i.e. represented in the basis functions which do not factorize into one-electron terms. This formalism accounts for all symmetries of the wave function present in atoms and enables straightforward handling of the matrix elements.

A. Many-electron angular factor

The angular part of the wave function is represented in terms of the modified solid harmonics, which are adapted here for use with explicitly correlated basis functions. We define the solid harmonics as

$$\mathcal{Y}_{LM}(\vec{r}) = \sqrt{4\pi} N_L r^L Y_{LM}(\hat{r}), \quad (17)$$

with some coefficients N_L to be determined, involving the standard spherical harmonics $Y_{LM}(\theta, \phi) \equiv Y_{LM}(\hat{r})$ with $\hat{r} = \vec{r}/r$. We recall the addition theorem for spherical harmonics

$$\frac{1}{2L+1} \sum_{M=-L}^L Y_{LM}^*(\hat{r}') Y_{LM}(\hat{r}) = \frac{1}{4\pi} P_L(\hat{r}' \cdot \hat{r}), \quad (18)$$

where P_L are the Legendre polynomials of the order L . The corresponding formula for the solid harmonics becomes

$$\frac{1}{2L+1} \sum_{M=-L}^L \mathcal{Y}_{LM}^*(\hat{r}') \mathcal{Y}_{LM}(\hat{r}) = A_L^2 r'^L r^L P_L(\hat{r}' \cdot \hat{r}) = (r'^{i_1} r'^{i_2} r'^{i_3} \dots r'^{i_L})^{(L)} (r^{i_1} r^{i_2} r^{i_3} \dots r^{i_L})^{(L)}, \quad (19)$$

where $(r^{i_1} r^{i_2} r^{i_3} \dots r^{i_L})^{(L)}$ is a traceless and symmetric tensor of the order L constructed from the vector \vec{r} with Cartesian indices $i_1, i_2, i_3, \dots, i_L$. The last equality in Eq. (19) determines the factor N_L , which is related to the coefficient of x^L in the Legendre polynomial $P_L(x)$, yielding

$$N_L^{-2} = \frac{1}{2^L} \binom{2L}{L}. \quad (20)$$

For example, $N_0 = 1$, $N_1 = 1$, $N_2 = \sqrt{2/3}$, $N_3 = \sqrt{2/5}$, and so on for consecutive L .

In the correlated wave function, the total angular momentum may come from an arbitrary electron or from an arbitrary combination of many electron angular momenta. Therefore, we introduce the following generalization of the solid harmonic

$$\begin{aligned} \mathcal{Y}_{LM}(\vec{\rho}_1, \vec{\rho}_2, \dots, \vec{\rho}_L) \\ \equiv \frac{1}{L!} (\vec{\rho}_1 \cdot \vec{\nabla}_r) (\vec{\rho}_2 \cdot \vec{\nabla}_r) \dots (\vec{\rho}_L \cdot \vec{\nabla}_r) \mathcal{Y}_{LM}(\vec{r}). \end{aligned} \quad (21)$$

Here, $\vec{\rho}_c$ stands for either an arbitrary single electron variable \vec{r}_a or for a cross product of any pair of electrons $\vec{r}_a \times \vec{r}_b$. Note that because of the L -fold differentiation, the right-hand side of Eq. (21) is r -independent. The function $\mathcal{Y}_{LM}(\vec{\rho}_1, \vec{\rho}_2, \dots, \vec{\rho}_L)$ is symmetric in all its arguments and has the variable overloading property $\mathcal{Y}_{LM}(\vec{r}, \vec{r}, \dots, \vec{r}) = \mathcal{Y}_{LM}(\vec{r})$. It also obeys the following summation rule

$$\begin{aligned} \frac{1}{2L+1} \sum_{M=-L}^L \mathcal{Y}_{LM}^*(\vec{\rho}_1', \vec{\rho}_2', \dots, \vec{\rho}_L') \mathcal{Y}_{LM}(\vec{\rho}_1, \vec{\rho}_2, \dots, \vec{\rho}_L) \\ = (\rho_1'^{i_1} \rho_2'^{i_2} \rho_3'^{i_3} \dots \rho_L'^{i_L})^{(L)} (\rho_1^{i_1} \rho_2^{i_2} \rho_3^{i_3} \dots \rho_L^{i_L})^{(L)}. \end{aligned} \quad (22)$$

This identity allows all the matrix elements to be expressed in terms of the scalar product, which is easy to handle with the explicitly correlated basis functions.

Let us start with the wave function having definite orbital and spin quantum numbers L and S and the corresponding projection quantum numbers M_L and M_S

$$\Psi^{LSM_L M_S} = \sum_n t_n \psi_n^{LSM_L M_S}, \quad (23)$$

where t_n are linear coefficients of the expansion. Each basis function $\psi_n^{LSM_L M_S}$ is an antisymmetrized product of a spatial and spin function

$$\psi^{LSM_L M_S} = \mathcal{A} \left[\phi_{LM_L}(\{\vec{r}_a\}) \chi_{\{a\}}^{SM_S} \right], \quad (24)$$

where the spatial function is a product of the generalized solid harmonic and a function ϕ that depends only on interparticle distances

$$\phi_{LM_L}(\{\vec{r}_a\}) = \mathcal{Y}_{LM_L}(\vec{\rho}_1, \vec{\rho}_2, \dots, \vec{\rho}_L) \phi(\{\vec{r}_a\}). \quad (25)$$

Let us now apply this formalism to the four-electron wave function of the beryllium atom and write explicitly the basis functions employed for atomic levels of different symmetry.

B. Four-electron basis functions

Let $\{a\}$ and $\{\vec{r}_a\}$ denote a sequence of electron indices 1, 2, 3, 4 and spatial coordinates $\vec{r}_1, \vec{r}_2, \vec{r}_3, \vec{r}_4$, respectively. A singlet state spin wave function χ^{SM_S} , for $\{a\}$ fixed at permutation (1, 2, 3, 4), has the form

$$\chi^{00} = \frac{1}{2}(\alpha_1 \beta_2 - \beta_1 \alpha_2)(\alpha_3 \beta_4 - \beta_4 \alpha_3) \quad (26)$$

and the corresponding triplet state functions are

$$\chi^{1-1} = \frac{1}{\sqrt{2}}(\alpha_1 \beta_2 - \beta_1 \alpha_2)\beta_3 \beta_4 \quad (27)$$

$$\chi^{10} = \frac{1}{2}(\alpha_1 \beta_2 - \beta_1 \alpha_2)(\alpha_3 \beta_4 + \beta_4 \alpha_3) \quad (28)$$

$$\chi^{11} = \frac{1}{\sqrt{2}}(\alpha_1 \beta_2 - \beta_1 \alpha_2)\alpha_3 \alpha_4. \quad (29)$$

In matrix elements of an arbitrary operator, all spin degrees of freedom can be reduced algebraically, see Sec. IV A, to a spin-free expression. Having this in mind and the summation rule Eq. (22), one can replace the basis functions ϕ_{LM_L} expressed in terms the solid harmonics by corresponding Cartesian basis functions

$$\phi^{i_1 \dots i_L} = (\rho_1^{i_1} \rho_2^{i_2} \rho_3^{i_3} \dots \rho_L^{i_L})^{(L)} \phi(\{\vec{r}_a\}), \quad (30)$$

where the variables ρ_c were defined beneath Eq. (21). Then, the spatial part of the basis function takes the following explicit forms:

– for S states

$$\phi_S \equiv \phi = \exp \left[- \sum_b \zeta_b r_b^2 - \sum_{c < d} \eta_{cd} r_{cd}^2 \right], \quad (31)$$

with the nonlinear parameters ζ and η determined variationally,

– for odd P states ($\vec{\rho}_1 = \vec{r}_p$)

$$\phi_P^i = r_p^i \phi; \quad (32)$$

– for even P states ($\vec{\rho}_1 = \vec{r}_p \times \vec{r}_q$)

$$\phi_{Pe}^i = \epsilon^{ijk} r_p^j r_q^k \phi, \quad (33)$$

where ϵ^{ijk} is the Levi-Civita symbol, and finally

– for even D states ($\vec{\rho}_1 = \vec{r}_p, \vec{\rho}_2 = \vec{r}_q$)

$$\phi_D^{ij} = \left(\frac{r_p^i r_q^j + r_p^j r_q^i}{2} - \frac{\delta^{ij}}{3} r_p^k r_q^k \right) \phi. \quad (34)$$

The subscripts p and q refer to arbitrary electrons (including the same ones), so that angular momentum may come from all the electrons in different combinations. A contribution to the expansion (23) from such different combinations can be optimized in a global minimization of the nonrelativistic energy.

In all matrix elements, the spin part is algebraically reduced and the angular part of the ϕ^{LM_L} function is converted into its Cartesian representation using the summation rule for solid harmonics of Eq. (22), so that the final formulas can all be represented in terms of simple reduced matrix elements, which are convenient to use with explicitly correlated functions. This spin reduction is described in the following section.

IV. MATRIX ELEMENTS

The matrix element of an arbitrary operator Q is

$$\langle \Psi | Q | \Psi \rangle = \sum_n \sum_m t_n^* t_m \langle \psi_n | Q | \psi_m \rangle \quad (35)$$

where we skipped the angular $LSM_L M_S$ or JM superscript over the wave function, because all formulas below will be independent on the angular representation of the wave function. The operator Q can adopt a variety of shapes according to nonrelativistic Hamiltonian and relativistic corrections. In the operator Q we can distinguish in general the spatial part O (scalar, vector, or tensor) and its spin part involving Pauli matrices σ . Below, we briefly describe the reduction of the matrix elements performed to get rid of the spin degrees of freedom. Such reduced matrix elements are assigned a double-braket symbol $\langle\langle \rangle\rangle$.

A. Reduction of the scalar matrix elements

Let us start from the spin independent operator O , for which

$$\langle \psi' | O | \psi \rangle = \hat{I} \langle\langle \phi' | O | \phi \rangle\rangle, \quad (36)$$

where \hat{I} denotes the identity operator in the angular momentum subspace. Namely, if we assume a JM representation, then

$$\langle \psi^{J'M'} | \psi^{JM} \rangle = \langle J'M' | JM \rangle \langle\langle \phi' | \phi \rangle\rangle. \quad (37)$$

The analogous formula holds for LM_L and SM_S representation, so Eq. (36) is independent of the angular momentum representation, as in all the formulas below in this subsection.

The reduced matrix element in Eq. (36) is defined by

$$\langle\langle \phi' | O | \phi \rangle\rangle = \langle \phi'(\{\vec{r}_a\}) | O \mathcal{A}[u_l \phi(\{\vec{r}_b\})] \rangle. \quad (38)$$

In the above expression \mathcal{A} denotes the sum over all $n!$ permutations of n electrons

$$\mathcal{A} = \sum_{l=1}^{n!} \varepsilon_l \mathcal{P}_l. \quad (39)$$

The coefficients

$$u_l = \varepsilon_l \langle \chi' | \hat{\Xi} \mathcal{P}_l \chi \rangle, \text{ with } \Xi = 1, \vec{\sigma}_a, \text{ or } \vec{\sigma}_a \vec{\sigma}_b, \quad (40)$$

which accompany the right function ϕ , depend on particular permutation \mathcal{P}_l and are explicitly shown for $n = 4$ in Table VII of Appendix B. The reduced matrix element may have implicit summation over Cartesian indices; then, $\langle\langle \phi' | O | \phi \rangle\rangle$ denotes $\langle\langle \phi'^i | O | \phi^i \rangle\rangle$ or $\langle\langle \phi'^{ij} | O | \phi^{ij} \rangle\rangle$ depending on the angular momentum of the state in question. We will skip these Cartesian indices as long as it does not lead to any confusion. These reduced matrix elements are a workhorse of this approach. For example, the matrix elements of the nonrelativistic Hamiltonian H can also be expressed in terms of the reduced ones. The fact that we originally did not use the wave function with specified J and M is irrelevant. The nonrelativistic Hamiltonian H does not depend on J or M , so different ψ^{LSJM} will lead to the same matrix elements as long as L and S are fixed.

B. Reduction of spin-dependent operators

Similarly, all the matrix elements of the spin-dependent operators in Eq. (6) can be expressed in terms of the reduced ones as follows

$$\langle \psi' | \sum_a \vec{\sigma}_a \cdot \vec{O}_a | \psi \rangle = -\frac{\vec{L} \cdot \vec{S}}{(L+1)} i \epsilon^{ijk} \sum_a \langle\langle \phi'^i | O_a^j | \phi^k \rangle\rangle_a, \quad (41)$$

$$\begin{aligned} \langle \psi' | \sum_{a < b} \sigma_a^i \sigma_b^j O_{ab}^{ij} | \psi \rangle &= \frac{12 (L^i L^j)^{(2)} (S^i S^j)^{(2)}}{(2L+3)(L+1)} \\ &\quad \times \sum_{a < b} \langle\langle \phi'^i | O_{ab}^{ij} | \phi^j \rangle\rangle_{ab}, \end{aligned} \quad (42)$$

where $\vec{S} = \frac{1}{2} \sum_a \vec{\sigma}_a$. Again, the angular indices of the wave function ψ are skipped because this angular part goes to matrix elements of $\vec{L} \cdot \vec{S}$ or $(L^i L^j)^{(2)} (S^i S^j)^{(2)}$ operators.

The above reduced matrix elements are defined as

$$\langle\langle \phi' | O_c | \phi \rangle\rangle_c = \langle\langle \phi'(\{\vec{r}_a\}) | O_c \mathcal{A}[u_l^c \phi(\{\vec{r}_b\})] \rangle\rangle, \quad (43)$$

$$\langle\langle \phi' | O_{cd} | \phi \rangle\rangle_{cd} = \langle\langle \phi'(\{\vec{r}_a\}) | O_{cd} \mathcal{A}[u_l^{cd} \phi(\{\vec{r}_b\})] \rangle\rangle, \quad (44)$$

and have the advantage that they involve only scalar operators built of spatial variables \vec{r}_a , and therefore they can all easily be evaluated in an explicitly correlated basis, in particular in the ECG basis. Moreover, these reduced matrix elements have the following properties

$$\sum_c \langle\langle \phi' | O | \phi \rangle\rangle_c = 2 \langle\langle \phi' | O | \phi \rangle\rangle, \quad (45)$$

$$\sum_{c < d} \langle\langle \phi' | O | \phi \rangle\rangle_{cd} = -\langle\langle \phi' | O | \phi \rangle\rangle, \quad (46)$$

which will be used to prove the above reduction formulas. For these proofs we shall need also the following two equalities

$$-i \epsilon^{ijk} \langle\langle \phi'^i | L^j | \phi^k \rangle\rangle = (L+1) \langle\langle \phi' | \phi \rangle\rangle, \quad (47)$$

$$\langle\langle \phi'^i | (L^i L^j)^{(2)} | \phi^k \rangle\rangle = -\frac{1}{6} (L+1) (2L+3) \langle\langle \phi' | \phi \rangle\rangle. \quad (48)$$

The reduction formulas are independent of the operator \vec{O}_a . So, to prove Eq. (41) let $\vec{O}_a = \vec{L}$ be the orbital angular momentum, then

$$l.h.s. = \langle \psi' | \sum_a \vec{\sigma}_a \cdot \vec{L} | \psi \rangle = \langle \psi' | 2 \vec{S} \cdot \vec{L} | \psi \rangle = 2 \vec{S} \cdot \vec{L} \langle\langle \phi' | \phi \rangle\rangle. \quad (49)$$

Using Eqs. (45) and (47), the right hand side of Eq. (41) can be rearranged to

$$\begin{aligned} r.h.s. &= -\frac{\vec{L} \cdot \vec{S}}{L+1} i \epsilon^{ijk} \sum_a \langle\langle \phi'^i | L^j | \phi^k \rangle\rangle_a \\ &= \frac{2}{L+1} \vec{L} \cdot \vec{S} (-i) \epsilon^{ijk} \langle\langle \phi'^i | L^j | \phi^k \rangle\rangle = 2 \vec{S} \cdot \vec{L} \langle\langle \phi' | \phi \rangle\rangle, \end{aligned} \quad (50)$$

which is equal to *l.h.s.* Similarly, to prove Eq. (42), let $O_{ab}^{ij} = (L^i L^j)^{(2)}$; then

$$l.h.s. = \langle \psi' | \sum_{a < b} \sigma_a^i \sigma_b^j (L^i L^j)^{(2)} | \psi \rangle$$

$$\begin{aligned} &= 2 \langle \psi' | S^i S^j (L^i L^j)^{(2)} | \psi \rangle \\ &= 2 (S^i S^j)^{(2)} (L^i L^j)^{(2)} \langle\langle \phi' | \phi \rangle\rangle. \end{aligned} \quad (51)$$

Taking Eq. (48), the right hand side of Eq. (42) becomes

$$\begin{aligned} r.h.s. &= -\frac{12 (L^i L^j)^{(2)} (S^i S^j)^{(2)}}{(2L+3)(L+1)} \langle\langle \phi'^i | (L^i L^j)^{(2)} | \phi^j \rangle\rangle \\ &= 2 (L^i L^j)^{(2)} (S^i S^j)^{(2)} \langle\langle \phi' | \phi \rangle\rangle, \end{aligned} \quad (52)$$

which is equal to *l.h.s.*

C. Reduction of the vector and tensor matrix elements

Analogous reductions can be performed for the hyperfine operators in H_{hfs} , namely

$$\langle \psi' | \sum_a \vec{\sigma}_a O_a | \psi \rangle = \vec{S} \sum_a \langle\langle \phi' | O_a | \phi \rangle\rangle_a, \quad (53)$$

$$\langle \psi' | \vec{O} | \psi \rangle = -\frac{\vec{L}}{(L+1)} i \epsilon^{ijk} \langle\langle \phi^i | O^j | \phi^k \rangle\rangle, \quad (54)$$

$$\langle \psi' | \sum_a \sigma_a^j O_a^{ij} | \psi \rangle = \frac{-6 S^j (L^i L^j)^{(2)}}{(2L+3)(L+1)} \sum_a \langle\langle \phi^i | O_a^{ij} | \phi^j \rangle\rangle_a, \quad (55)$$

$$\langle \psi' | O^{ij} | \psi \rangle = \frac{-6 (L^i L^j)^{(2)}}{(2L+3)(L+1)} \langle\langle \phi^i | O^{ij} | \phi^j \rangle\rangle. \quad (56)$$

The proofs of the above reduction formulas are very similar to those shown in the preceding subsection. One assumes that $O_a = \hat{I}$, $\vec{O} = \vec{L}$, $O_{ab}^{ij} = (L^i L^j)^{(2)}$, and repeats the previous proofs correspondingly.

V. EFFECTIVE FINE/HYPERFINE HAMILTONIAN

In order to account for the combined fine and hyperfine structure with an arbitrary coupling strength, it is necessary to extend the original formulation of the hyperfine splitting theory by Hibbert [58] and represent the fine and the hyperfine structure of an arbitrary state in terms of an effective Hamiltonian, instead of expectation values. The effective Hamiltonian reads

$$\begin{aligned} H_{\text{eff}} &= c_0 + c_1 \vec{L} \cdot \vec{S} + c_2 (L^i L^j)^{(2)} (S^i S^j)^{(2)} \\ &\quad + a_1 \vec{I} \cdot \vec{S} + a_2 \vec{I} \cdot \vec{L} + a_3 (L^i L^j)^{(2)} S^i I^j \\ &\quad + \frac{b}{6} \frac{3 (I^i I^j)^{(2)}}{I (2I-1)} \frac{3 (L^i L^j)^{(2)}}{L (2L-1)}, \end{aligned} \quad (57)$$

where the coefficients $a_1, a_2, a_3, b, c_0, c_1$, and c_2 are independent of $\vec{J} = \vec{L} + \vec{S}$ but are specific to the particular state. The c_0 coefficient is the so-called centroid energy, which in our case is

$$c_0 = E_0 + E_{\text{ns}}^{(4)} + \mathcal{O}(\alpha^5), \quad (58)$$

where $E_{\text{ns}}^{(4)} = \langle H_{\text{ns}}^{(4)} \rangle$ is the spin-independent relativistic correction. This correction can be rewritten as

$$E_{\text{ns}}^{(4)} = -\frac{1}{8}V_1 + \frac{Z}{8}V_2 + \frac{1}{4}V_3 - \frac{1}{2}V_4 + \frac{Z}{2m_N}V_5, \quad (59)$$

with V_1, \dots, V_5 defined in Table II. The fine structure parameters c_1 and c_2 , using formulas from the previous section, are

$$c_1 = -\frac{1}{(L+1)} \left[\frac{Z}{4} \left((g-1)V_{f1} - \frac{g}{m_N}V_{f4} \right) + \frac{1}{4} \left(gV_{f2} - (g-1)V_{f3} \right) \right], \quad (60)$$

$$c_2 = -\frac{12}{(2L+3)(L+1)} \frac{3g^2}{16} V_{f5}, \quad (61)$$

while the hyperfine structure parameters are

$$a_1 = \frac{Z}{m_N} \frac{gg_N}{12} V_{h1}, \quad (62)$$

$$a_2 = -\frac{1}{(L+1)} \frac{Z}{m_N} \left(\frac{g_N}{2} V_{h2} - \frac{g_N-1}{2m_N} V_{h3} \right), \quad (63)$$

$$a_3 = \frac{-6}{(2L+3)(L+1)} \frac{Z}{m_N} \frac{3gg_N}{8} V_{h4}, \quad (64)$$

$$b = \frac{6L(2L-1)}{(2L+3)(L+1)} Q_N V_{h5}. \quad (65)$$

The expectation values V_{fi} and V_{hi} used to determine the fine and hyperfine parameters are defined in Table III. Once these parameters are calculated, the effective hyperfine structure Hamiltonian H_{eff} can be diagonalized, for example in the $|L, M_L; S, M_S; I, M_I\rangle$ basis, yielding the combined fine/hyperfine levels with respect to the centroid energy c_0 .

VI. CALCULATIONS AND RESULTS

A. Centroid energies

1. Variational optimization of the nonrelativistic energy

In the numerical calculations we followed closely our previous works devoted to the singlet S and P states of beryllium [39, 40]. We used the wave functions expanded in the basis of ECG functions (31)-(34), whose non-linear parameters were variationally optimized. The optimization was performed at the infinite nuclear mass limit of the nonrelativistic Hamiltonian, Eq. (3). Then, the nonrelativistic energies and the wave functions of ${}^9\text{Be}$ were generated with the same nonlinear parameters without significant loss of accuracy. In order to achieve numerical accuracy $\sim 10^{-9}$ for nonrelativistic energy E_0 , which is equivalent to a numerical accuracy of energy levels $< 0.01 \text{ cm}^{-1}$, we assumed the maximum size of the basis sets equal to 4096, 6144, and 8192 for S -, P -, and D -states, respectively. A sequence of energies obtained for consecutive basis sets enabled extrapolation to the complete

basis limit and estimation of the error resulting from basis set truncation. The nonrelativistic energy E_0 convergence for all the studied states of ${}^{\infty}\text{Be}$ is presented in Table I. Note that the rate of the convergence depends on the given atomic state.

This table contains also the best currently available literature results. For the $2s3s\,{}^3S$ state the energy reported by Frolov and Wardlaw [59] seems to be rather poorly converged—despite using a 7000-term ECG expansion their result is about $8 \cdot 10^{-6}$ a.u. $\approx 2 \text{ cm}^{-1}$ above our energy obtained with 4096-term wave function. Significantly longer ECG expansions have been employed for the $2s2p\,{}^1P$, $2s2p\,{}^3P$, and $2p^2\,{}^1D$ states by Adamowicz *et al.* [42, 43, 61]. In these cases, their variational energy is by $10^{-8} - 10^{-9}$ a.u. lower than our upper bound, whereas for the $2s3d\,{}^3D$ state our upper bound slightly improves over the variational energy obtained by Sharkey *et al.* [41] from an equivalent ECG expansion. The best previous calculations of the nonrelativistic energy for the $2p^2\,{}^3P$ state were obtained using a full-core plus correlation (FCPC) method [60] and gave the energy almost 5 cm^{-1} higher than the current one.

In general, the current state-of-the-art calculations offer a relative accuracy of the order of 10^{-10} , which corresponds to $\approx 10^{-4} \text{ cm}^{-1}$ of absolute accuracy. Still, there seems to be room for further accuracy improvement of the ECG method in relation to four-electron atoms, either by increasing the basis size or by tuning the optimization algorithms. However, the ability to maintain reliable numerical convergence is limited due to the double precision arithmetic used in the algorithms. Significant improvement of the current results will require the use of higher precision arithmetic and bases of size > 20000 , which means a dramatic increase in the computation time. This suggests the need to redesign current ECG algorithms or look for new, more efficient solutions in the future.

2. Calculations of reduced matrix elements

The finite-mass wave functions were subsequently employed in the evaluation of matrix elements. The values of all the reduced matrix elements for relativistic and QED corrections along with the nonrelativistic energy and the Bethe logarithm are collected in Tables II, III. All the entries represent extrapolated values with estimated uncertainty. Because the use of original formulas for singular operators leads to a slow numerical convergence (this spurious effect is particularly exposed in calculations using Gaussian-type basis functions having improper short-distance behavior), regularized versions of matrix elements were employed following the rules provided in Appendix A. For the $2s2p\,{}^1P$ state the Bethe logarithm, $\ln k_0$, was calculated directly in Ref. 39, and in this case the overall uncertainty is dominated by the higher order corrections. This numerical value of $\ln k_0$ was adopted also for the remaining states with a relevantly large uncertainty assigned. Eventually, this uncertainty dominated the overall theoretical uncertainty. The centroid energies evaluated with these matrix elements are put together in Table IV.

TABLE I. Convergence of the nonrelativistic energy E_0 of ${}^{\infty}\text{Be}$ (in a.u.) and comparison with other ECG results, or if not available, with the most accurate value from another method.

Size	$2s3s\,{}^3S$	Size	$2s2p\,{}^1P$	Size	$2s2p\,{}^3P$
768	-14.430 065 800 88	1024	-14.473 445 215 92	1024	-14.567 241 485 35
1024	-14.430 066 834 12	1536	-14.473 449 010 68	1536	-14.567 243 359 33
1536	-14.430 067 459 90	2048	-14.473 450 455 64	2048	-14.567 243 913 64
2048	-14.430 067 579 18	3072	-14.473 451 162 07	3072	-14.567 244 114 67
3072	-14.430 067 637 28	4096	-14.473 451 310 50	4096	-14.567 244 192 08
4096	-14.430 067 666 35	6144	-14.473 451 361 77	6144	-14.567 244 215 84
∞	-14.430 067 678(7)	∞	-14.473 451 384(9)	∞	-14.567 244 232(8)
[59] 7000	-14.430 059 43	[42] 16400	-14.473 451 388 2	[43] 8000	-14.567 244 222
Size	$2p^2\,{}^3P^e$	Size	$2p^2\,{}^1D$	Size	$2s3d\,{}^3D$
1024	-14.395 452 640 71	1536	-14.408 232 496 49	1536	-14.384 631 192 32
1536	-14.395 453 441 97	2048	-14.408 234 916 82	2048	-14.384 632 963 77
2048	-14.395 453 625 95	3072	-14.408 236 788 28	3072	-14.384 633 859 38
3072	-14.395 453 700 13	4096	-14.408 237 032 51	4096	-14.384 634 414 54
4096	-14.395 453 720 27	6144	-14.408 237 213 69	6144	-14.384 634 572 57
6144	-14.395 453 738 26	8192	-14.408 237 270 12	8192	-14.384 634 603 77
∞	-14.395 453 745(4)	∞	-14.408 237 290(9)	∞	-14.384 634 616(7)
[60] FCPC	-14.395 431 6	[61] 12300	-14.408 237 282	[41] 8100	-14.384 634 597 13

TABLE II. Expectation values of various operators and spin-independent reduced matrix elements of ${}^9\text{Be}$ (in a.u.).

Reduced matrix element	$2s3s\,{}^3S$	$2s2p\,{}^1P$	$2p^2\,{}^1D$
E_0	-14.429 160 970(6)	-14.472 543 762(11)	-14.407 351 381(10)
$V_1 = \sum_a \langle\langle \vec{p}_a^4 \rangle\rangle$	2 149.4858(8)	2 132.7877(18)	2 109.0093(9)
$V_2 = \sum_a \langle\langle 4\pi \delta^3(r_a) \rangle\rangle$	441.618 01(6)	438.458 40(4)	434.113 91(8)
$V_3 = \sum_{a < b} \langle\langle 4\pi \delta^3(r_{ab}) \rangle\rangle$	19.904 846(4)	19.700 026(7)	19.370 006(5)
$V_4 = \sum_{a < b} \langle\langle p_a^i \left(\frac{\delta^{ij}}{r_{ab}} + \frac{r_a^i r_b^j}{r_{ab}^3} \right) p_b^j \rangle\rangle$	1.814 877(4)	1.622 713(4)	1.380 895 6(5)
$V_5 = \sum_a \langle\langle p_a^i \left(\frac{\delta^{ij}}{r_a} + \frac{r_a^i r_a^j}{r_a^3} \right) p_N^j \rangle\rangle$	-223.060 24(2)	-220.643 672(2)	-217.444 43(3)
$\ln k_0$	5.752(3) ^a	5.752 32(8) ^a	5.752(3) ^a
$\sum_{a < b} \langle\langle P(r_{ab}^{-3}) \rangle\rangle$	-7.486 93(2) ^b	-7.097 17(3) ^b	-6.918 15(2) ^b
$V_{h1} = \sum_a \langle\langle 4\pi \delta^3(r_a) \rangle\rangle_a$	13.294 900(10)		
$V_{h2} = i \epsilon^{ijk} \sum_a \langle\langle i \left(\frac{\vec{r}_a}{r_a^3} \times \vec{p}_a \right)^j k \rangle\rangle$		-0.370 894(3)	-0.559 374 9(18)
$V_{h3} = i \epsilon^{ijk} \sum_a \langle\langle i \left(\frac{\vec{r}_a}{r_a^3} \times \vec{p}_N \right)^j k \rangle\rangle$		-0.112 512(9)	-0.216 094(3)
$V_{h5} = \sum_a \langle\langle i \left \frac{r_a^i r_a^j}{r_a^5} - \frac{\delta^{ij}}{3 r_a^3} \right j \rangle\rangle$		0.112 086 0(11)	0.080 872 8(12)

^a Adopted from $2s2p\,{}^1P$ state [39]; ^b Calculated in the infinite mass limit. ^c [39];

B. Combined fine/hyperfine structure

The effective Hamiltonians of the general form given by Eq. (57) were constructed separately for each atomic state. They differ from each other in numerical values of parameters a_1 , a_2 , a_3 , b , c_1 , and c_2 , listed in Table V, and hence also in the number of terms included. These Hamiltonians were diagonalized in the basis of $|L, M_L; S, M_S; I, M_I\rangle$ states using standard angular momentum algebra. Numerical eigenvalues representing the shift of the atomic hyperfine level with respect to the corresponding centroid are presented in Table VI.

Depending on the atomic state, these hyperfine levels extend in the range from tens up to almost a hundred thousand MHz. Figures 2-4 show graphically the fine/hyperfine splitting in the case of three angular momenta states. The corresponding eigenfunctions, in turn, can be employed to provide intensities of transitions between individual hyperfine levels and help to overcome the line-shape-related limitations to the precision of contemporary measurements [44, 46].

Because the states 3S_1 , 1P_1 , and 1D_2 involve only two angular momenta, one can employ the commonly used A_J and

TABLE III. Expectation values of various operators and spin-independent reduced matrix elements of ${}^9\text{Be}$ (in a.u.).

Reduced matrix element	$2s2p\,{}^3P$	$2p^2\,{}^3P^e$	$2s3d\,{}^3D$
E_0	-14.566 341 475(4)	-14.394 568 519(5)	-14.383 731 170(6)
$V_1 = \sum_a \langle\langle \vec{p}_a^4 \rangle\rangle$	2 131.397 1(15)	2 086.304 2(12)	2 144.482 7(7)
$V_2 = \sum_a \langle\langle 4\pi \delta^3(r_a) \rangle\rangle$	438.127 79(11)	429.777 10(13)	440.786 59(9)
$V_3 = \sum_{a < b} \langle\langle 4\pi \delta^3(r_{ab}) \rangle\rangle$	19.684 698(3)	19.065 685(2)	19.837 514(2)
$V_4 = \sum_{a < b} \langle\langle p_a^i \left(\frac{\delta^{ij}}{r_{ab}} + \frac{r_{ab}^i r_{ab}^j}{r_{ab}^3} \right) p_b^j \rangle\rangle$	1.457 377 9(16)	1.070 998 2(13)	1.809 602 7(12)
$V_5 = \sum_a \langle\langle p_a^i \left(\frac{\delta^{ij}}{r_a} + \frac{r_a^i r_a^j}{r_a^3} \right) p_N^j \rangle\rangle$	-220.376 91(6)	-214.225 93(5)	-222.412 27(6)
$\ln k_0$	5.752(3) ^a	5.752(3) ^a	5.752(3) ^a
$\sum_{a < b} \langle\langle P(r_{ab}^{-3}) \rangle\rangle$	-6.966 49(3) ^b	-6.505 54(4) ^b	-7.493 48(2) ^b
$V_{f1} = i \epsilon^{ijk} \sum_a \langle\langle i \left(\frac{\vec{r}_a}{r_a^3} \times \vec{p}_a \right)^j k \rangle\rangle_a$	-0.605 451(3)	-0.620 435 4(7)	-0.016 199 88(6)
$V_{f2} = i \epsilon^{ijk} \sum_a \sum_{b \neq a} \langle\langle i \left(\frac{\vec{r}_{ab}}{r_{ab}^3} \times \vec{p}_b \right)^j k \rangle\rangle_a$	0.273 149 3(4)	0.296 033 6(2)	0.010 830 7(4)
$V_{f3} = i \epsilon^{ijk} \sum_a \sum_{b \neq a} \langle\langle i \left(\frac{\vec{r}_{ab}}{r_{ab}^3} \times \vec{p}_a \right)^j k \rangle\rangle_a$	-1.124 565(4)	-1.154 002 9(3)	-0.040 076 2(5)
$V_{f4} = i \epsilon^{ijk} \sum_a \langle\langle i \left(\frac{\vec{r}_a}{r_a^3} \times \vec{p}_N \right)^j k \rangle\rangle_a$	-0.243 575 3(2)	-0.187 062 4(12)	0.003 014 1(4)
$V_{f5} = \sum_{a < b} \langle\langle i \left(\frac{r_{ab}^i r_{ab}^j}{r_{ab}^5} - \frac{\delta^{ij}}{3r_{ab}^3} \right) j \rangle\rangle_{ab}$	-0.017 082 4(3)	0.012 571 98(2)	-0.000 828 213(2)
$V_{h1} = \sum_a \langle\langle 4\pi \delta^3(r_a) \rangle\rangle_a$	9.247 623(18)	-1.389 667(5)	12.130 05(3)
$V_{h2} = i \epsilon^{ijk} \sum_a \langle\langle i \left(\frac{\vec{r}_a}{r_a^3} \times \vec{p}_a \right)^j k \rangle\rangle$	-0.606 202(3)	-0.621 281 1(7)	-0.016 209 10(9)
$V_{h3} = i \epsilon^{ijk} \sum_a \langle\langle i \left(\frac{\vec{r}_a}{r_a^3} \times \vec{p}_N \right)^j k \rangle\rangle$	-0.240 311(8)	-0.237 269(4)	0.003 328 5(8)
$V_{h4} = \sum_a \langle\langle i \left(\frac{r_a^i r_a^j}{r_a^5} - \frac{\delta^{ij}}{3r_a^3} \right) j \rangle\rangle_a$	0.219 150 1(6)	-0.218 683 3(9)	0.002 441(2)
$V_{h5} = \sum_a \langle\langle i \left(\frac{r_a^i r_a^j}{r_a^5} - \frac{\delta^{ij}}{3r_a^3} \right) j \rangle\rangle$	0.192 574 73(18)	-0.194 530 5(4)	0.002 083(2)

^a Adopted from $2s2p\,{}^1P$ state [39]; ^b Calculated in the infinite mass limit.

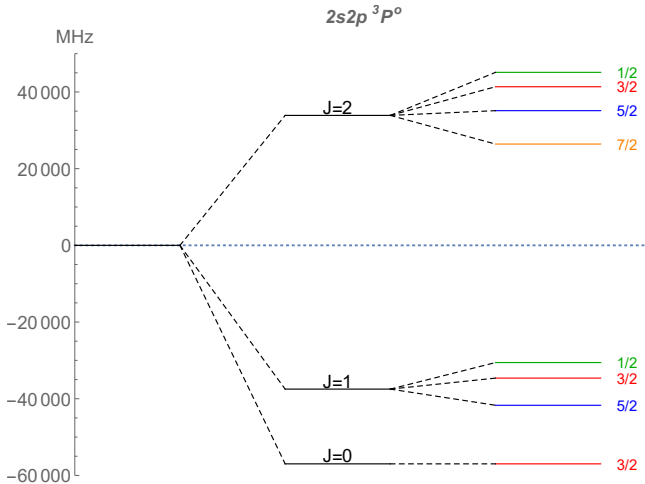


FIG. 2. The fine and hyperfine splitting for the $2s2p\,{}^3P^o$ state. The hf splitting was scaled by a factor of 20.

B_J coefficients to represent their hyperfine structure

$$\langle H_{\text{hfs}} \rangle_J = A_J \vec{I} \cdot \vec{J} + \frac{B_J}{6} \frac{3(I^i I^j)^{(2)}}{I(2I-1)} \frac{3(J^i J^j)^{(2)}}{J(2J-1)}, \quad (66)$$

where \vec{J} is the total electronic angular momentum. So, in the

case of the $2s3s\,{}^3S_1$ state, $\vec{J} = \vec{S}$ and

$$A_1({}^3S) = a_1 (1 + \epsilon) = -332.50(2) \text{ MHz} \quad (67)$$

$$B_1({}^3S) = 0, \quad (68)$$

where $\epsilon = 0.654 \times 10^{-3}$ was taken from Ref. [9]. In the case of the $2s2p\,{}^1P_1$ state, $\vec{J} = \vec{L}$ and

$$A_1({}^1P) = a_2 = -13.888 2(7) \text{ MHz} \quad (69)$$

$$B_1({}^1P) = b = 0.845 40(4) \text{ MHz}. \quad (70)$$

Finally for the $2p^2\,{}^1D_2$ state, $\vec{J} = \vec{L}$ and

$$A_2({}^1D) = a_2 = -13.964 0(7) \text{ MHz} \quad (71)$$

$$B_2({}^1D) = b = 1.742 80(9) \text{ MHz}. \quad (72)$$

The calculation of the fine/hyperfine structure for the $2s2p\,{}^3P$, $2p^2\,{}^3P^e$, and $2s3d\,{}^3D$ states requires diagonalization of the effective fine/hyperfine Hamiltonian in Eq. (57). For the $2s3d\,{}^3D$ state, the diagonalization reveals that the a_1 parameter is around three times larger than the parameters c_1 and c_2 . This makes the interaction of electronic and nuclear spins the dominating one and disqualifies J as a good quantum number. Therefore, one cannot use A_J and B_J coefficients—instead we present actual values of the fine/hyperfine levels. In addition, to account for the leading relativistic and radiative corrections, the a_1 parameter is rescaled by the $(1 + \epsilon)$ factor, see Eq. (67) and the related discussion in Sec. II C 2.

TABLE IV. Centroid energy contributions (in cm^{-1}) relative to the ground $2s^2 1S$ state for ${}^9\text{Be}$ and comparison with experimental and other theoretical data. The total energy in terms of the ionization potential is also shown at the bottom of the table.

	$2s2p\ 3P$	$2s2p\ 1P$	$2s3s\ 3S$	$2p^2\ 1D$	$2p^2\ 3P^e$	$2s3d\ 3D$
$m\alpha^2$	21 968.103(3)	42 554.325(6)	52 075.750(10)	56 862.395(5)	59 667.912(2)	62 046.433(3)
$m\alpha^4$	13.189(3)	12.171(3)	5.726(4)	21.968(4)	30.728(4)	8.000(5)
$m\alpha^5$	-1.06(4)	-1.0106(10)	-0.46(7)	-1.73(5)	-2.46(5)	-0.61(5)
$m\alpha^6$	-0.048(10)	-0.045(9)	-0.021(5)	-0.08(2)	-0.11(3)	-0.027(7)
Total	21 980.18(5)	42 565.441(11)	52 080.99(7)	56 882.55(6)	59 696.07(6)	62 053.79(6)
Theory (ECG)	21 979.4(11) ^e					
Theory (FCPC) ^f	21 980.85	42 568.80	52 081.09	56 890.9	59 699.8	62 055.25
Theory (MCHF) ^h	22 099.30	42 710.97	52 080.09	56 945.89	59 793.35	62 165.91
Experiment	21 980.16(8) ^{a,g}	42 565.4502(10) ^b	52 080.94(6) ^a	56 882.5474(21) ^c	59 696.07(5) ^{a,g}	62 053.74(6) ^{a,g}
Total – Experiment ^d	0.02(5)	-0.009(11)	0.05(7)	0.00(6)	0.04(6)	0.05(6)
Total (ionization)	53 212.51(5)	32 627.265(11)	23 111.73(5)	18 310.13(5)	15 496.62(6)	13 138.90(5)
Theory(FCPC) ^f	53 211.22	32 623.27	23 110.98			13 136.8

^a Johansson [62], Kramida *et al.* [49]; ^b Cook *et al.* [44]; ^c Cook *et al.* [46]; ^d Theoretical uncertainty assumed.; ^e Kedzierski *et al.* [43], averaged over J ; ^f Chung and Zhu [60, 63]; ^g Centroid uncertainty taken as the maximum error from the individual J lines.; ^h Froese Fischer and Tachiev [64].

C. Comparison with experimental and other theoretical results

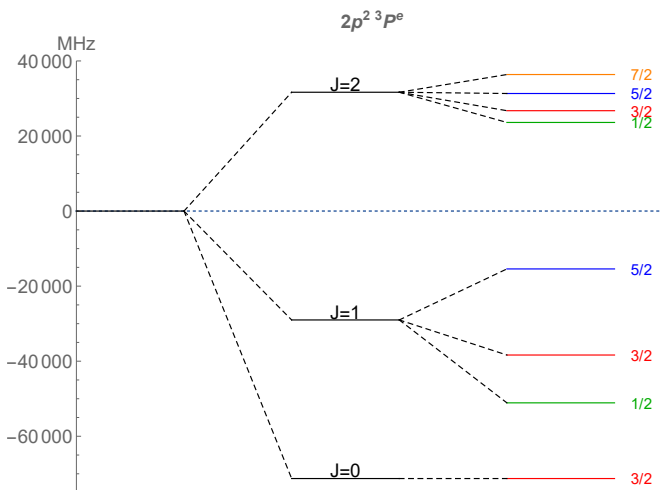


FIG. 3. The fine and hyperfine splitting for the $2p^2\ 3P^e$ state. The hf splitting was scaled by a factor of 500.

Table IV presents our recommended total energies of centroids and their components of Eq. (1). The energy of the ground $2s^2 1S$ level was taken as a reference for the wavenumber scale. The extrapolated values and uncertainties of the nonrelativistic contribution (see Table I) and of all the corrections were estimated from their convergence with increasing size of basis sets. As can be inferred from the table, except for the $2s2p\ 1P$ state, that the accuracy of the total energy is limited mainly by the uncertainty of the leading QED correction. This correction is dominated by the Bethe logarithm

term, which is estimated using $\ln k_0 = 5.752(3)$ [39].

The total energy of a centroid for all the six states considered here is consistent within the theoretical uncertainty with the experimental one [44, 46, 49, 62]—see ‘Total – Experiment’ entries in Table IV. The agreement is on the level of 0.01 cm^{-1} . In particular, our predictions agree with order-of-magnitude more accurate measurements reported by Williams group [44, 46]. For the $2p^2\ 3P^e$ term, there is a small difference between the original triplet ($J = 0, 1, 2$) wavenumbers by Johansson [62] and those reported on the NIST web page [49], which affects the centroid values. The experimental value placed in Table IV refers to original measurements and we note that value from the NIST compilation is smaller by 0.09 cm^{-1} .

There are also scarce theoretical data in the literature concerning selected excited states of ${}^9\text{Be}$. Chung and Zhu [60, 63] evaluated the energy using the FCPC method and included the relativistic and QED correction but without the uncertainty estimation, see Table IV. Their centroid energies differ from ours and from the experimental ones by 0.1 to 3.4 cm^{-1} . Much newer results obtained by Froese Fisher and Tachiev using a multiconfiguration Hartree-Fock (MCHF) [64] method differ from ours by as much as 63 – 146 cm^{-1} with the exception of the 3S level ($\sim 1\text{ cm}^{-1}$). The centroid energy of the $2s2p\ 3P$ state obtained from Kedzierski’s calculations [43], being less accurate, agrees within the uncertainty with our result. Surprisingly, their relativistic correction $12.40(7)\text{ cm}^{-1}$ is in significant disagreement with our value of $13.189(3)\text{ cm}^{-1}$. The difference between these two values corresponds to the difference between their centroid energy and the experimental one, and thus raises doubts about their uncertainty estimation.

Fine-structure splittings obtained theoretically and experimentally for both 3P terms agree well with each other. Sep-

parate comment is required concerning the $2s3d\ ^3D$ term. Its fine-structure has not been revealed in Johansson's experiments [62]. Even then, it has been given on the NIST page [49]. The fine splitting has also been predicted theoretically by Chung and Zhu [63] and by Froese Fisher and Tachiev [64]. However, in view of the clear domination of the IS over LS coupling (see discussion in Sec. VI B), we claim that for this term the notion of the fine-structure should be either totally abandoned or at least reinterpreted in terms of the $\vec{K} = \vec{I} + \vec{S}$ angular momentum (see Fig. 4).

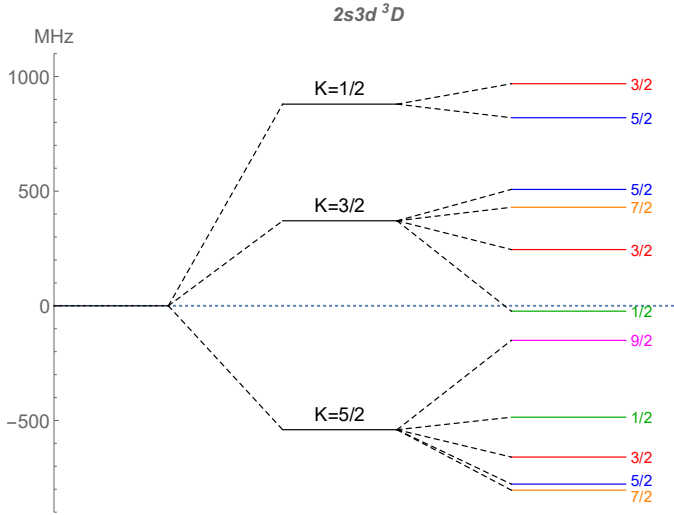


FIG. 4. The fine and hyperfine splitting for the $2s3d\ ^3D$ state. The angular momentum number K , defined as $\vec{K} = \vec{I} + \vec{S}$, is an approximate quantum number.

VII. CONCLUSIONS

We have performed the most accurate calculations of centroid energies and fine/hyperfine structure parameters of low lying ${}^1,{}^3P_J$, 3S_1 , ${}^3P_J^e$, and ${}^1,{}^3D_J$ excited states of the ${}^9\text{Be}$ atom. The obtained results, apart from being in agreement with available experimental values, allow the accuracy of standard atomic structure calculations to be assessed. For a long time, the FCPC method by Chung and Zhu [63] was considered the most accurate one regarding the centroid energies which included the finite nuclear mass, relativistic, and QED corrections. However, significant differences between the FCPC results and our calculations (and experiments), reaching several reciprocal centimeters (up to 8 cm^{-1} for the 1D state), show the importance of the use of high-quality wave functions in accurate studies of the atomic structure. It is noteworthy that these differences are often greater than the entire QED correction. What is more, some of the previous calculations of the combined fine and hyperfine structure were performed incorrectly. The reason was that the LS coupling was assumed to be dominant over all other couplings. In other words, we demonstrated that the standard approach in terms of A_J and B_J hyperfine parameters does not work for some

${}^9\text{Be}$ excited states, and that a subtle analysis is necessary to properly identify the origin of energy level splitting.

Apart from presenting accurate results for the fine and hyperfine structure, we have introduced an approach allowing us to handle the combined fine and hyperfine structure of an arbitrary atomic system in terms of an effective Hamiltonian. This Hamiltonian is to be diagonalized for particular values of the fine/hyperfine coupling parameters. This approach is particularly suitable in cases where the hyperfine mixing becomes significant. Moreover, we expressed the fine and hyperfine parameters in terms of reduced matrix elements with Cartesian angular factors. These factors can conveniently be combined with a general correlated basis function and applied to an arbitrary atomic term.

The current capabilities of theoretical methods are limited by the accuracy of both $m\alpha^5$ and $m\alpha^6$ QED components. As shown by the instance of the $2s2p\ ^1P$ state, more accurate calculations of the former component are feasible, but, significantly more effort will be needed to evaluate accurately the latter component. Its complete evaluation will require construction of wave functions strictly obeying the cusp condition as it has already been demonstrated for two-electron systems [57, 65].

ACKNOWLEDGMENTS

Fruitful exchange of information with Alexander Kramida is acknowledged. This research was supported by National Science Center (Poland) Grants No. 2014/15/B/ST4/05022, 2019/34/E/ST4/00451 and 2017/27/B/ST2/02459, as well as by a computing grant from Poznań Supercomputing and Networking Center and by PL-Grid Infrastructure.

Appendix A: Regularization

This appendix briefly describes the regularization technique of singular operators used in this work. We can assume that a operator Q to be regularized depends only on a two-particle coordinate \vec{r}_{aX} , i.e. electron-nucleus $Q = Q(\vec{r}_a) \equiv Q(\vec{r}_{aN})$, $X = N$ or electron-electron $Q = Q(\vec{r}_{ab})$, $X = b$.

For any operator Q , one finds a corresponding operator \tilde{Q} , such that

$$\begin{aligned} \left(\frac{1}{m} + \frac{1}{m_X} \right) Q &= \frac{1}{m_N} [\vec{p}_N, [\vec{p}_N, \tilde{Q}]] + \frac{1}{m} \sum_c [\vec{p}_c, [\vec{p}_c, \tilde{Q}]] \\ &= [Q]_r - 2 \{ E_0 - H^{(2)}, \tilde{Q} \}, \end{aligned} \quad (\text{A1})$$

where the curly bracket denotes an anticommutator and

$$[Q]_r = 4(E_0 - V)\tilde{Q} - \sum_c \vec{p}_c \tilde{Q} \vec{p}_c - \frac{1}{m_N} \vec{p}_N \tilde{Q} \vec{p}_N. \quad (\text{A2})$$

Using the above notation, an expectation value of a one-electron operator $Q = Q(\vec{r}_a)$ can be represented in the regularized form as

$$\langle \Psi | Q | \Psi \rangle = \left(\frac{1}{m} + \frac{1}{m_X} \right)^{-1} \langle \Psi | [Q]_r | \Psi \rangle \quad (\text{A3})$$

TABLE V. The nonrelativistic energy and theoretical fine and hyperfine structure parameters for the $2s2p\ ^3P$ state of ${}^9\text{Be}$ (in MHz). Nuclear mass $m_N = 9.01218307(8)$ u [18], magnetic moment $\mu/\mu_N = -1.177432(3)$ [8], and quadrupole moment $Q_N = 0.05350(14)$ barns [9] were used for the ${}^9\text{Be}$ nucleus. The a_1 coefficient is to be multiplied by $1 + \epsilon$ according to Eq. (16). Shown uncertainties are of the numerical origin, while implicit relative uncertainties due to unknown relativistic corrections are about α^2

State	c_1	c_2	a_1	a_2	a_3	b/Q_N (MHz/barn)
$2s3s\ ^3S$			-332.283 4(3)			
$2s2p\ ^1P$				-13.888 28(8)		15.801 75(7)
$2s2p\ ^3P$	32 987.6(2)	5 399.15(2)	-231.128 4(6)	-22.699 24(5)	14.788 68(5)	27.148 87(3)
$2p^2\ ^3P^e$	32 321.08(9)	-3 973.643(4)	34.732 27(8)	-23.263 96(15)	-14.757 164(4)	-27.424 71(4)
$2p2p\ ^1D$				-13.963 93(3)		32.575 5(3)
$2s3d\ ^3D$	90.400(9)	124.654 6(2)	-303.169 8(6)	-0.404 656 7(15)	0.078 38(7)	0.838 9(6)

TABLE VI. Fine/hyperfine levels (in MHz) of low lying excited states of ${}^9\text{Be}$ atom. $\vec{J} = \vec{L} + \vec{S}$, $\vec{K} = \vec{I} + \vec{S}$, $\vec{F} = \vec{L} + \vec{S} + \vec{I}$. The numerical uncertainty is negligible, while the implicit relative uncertainty due to unknown higher order relativistic corrections is about α^2 .

$\nu_J(F)$	$2s2p\ ^3P$	$2p^2\ ^3P^e$	$\nu_K(F)$	$2s3d\ ^3D$
$\nu_0(3/2)$	-56 982.	-71 265.	$\nu_{1/2}(3/2)$	968.54
$\nu_1(1/2)$	-37 697.	-29 054.	$\nu_{1/2}(5/2)$	820.31
$\nu_1(3/2)$	-37 343.	-29 028.	$\nu_{3/2}(1/2)$	-23.38
$\nu_1(5/2)$	-37 140.	-28 983.	$\nu_{3/2}(3/2)$	245.25
$\nu_2(1/2)$	33 514.	31 643.	$\nu_{3/2}(5/2)$	507.55
$\nu_2(3/2)$	33 950.	31 649.	$\nu_{3/2}(7/2)$	429.71
$\nu_2(5/2)$	34 262.	31 658.	$\nu_{5/2}(1/2)$	-485.73
$\nu_2(7/2)$	34 449.	31 668.	$\nu_{5/2}(3/2)$	-659.71
			$\nu_{5/2}(5/2)$	-777.63
			$\nu_{5/2}(7/2)$	-803.93
			$\nu_{5/2}(9/2)$	-150.57
$\nu_J(F)$	$2s2p\ ^1P_1$	$2s3s\ ^3S_1$	$\nu_J(F)$	$2p^2\ ^1D_2$
$\nu_1(1/2)$	35.777	831.25	$\nu_2(1/2)$	64.363
$\nu_1(3/2)$	13.043	332.50	$\nu_2(3/2)$	41.892
$\nu_1(5/2)$	-20.621	-498.75	$\nu_2(5/2)$	5.893
			$\nu_2(7/2)$	-41.456

There are two one-electron operators, i.e. $4\pi\delta^3(r_a)$ and $r_a^{-5}(r_a^i r_a^j - 1/3\delta^{ij}r_a^2)$, and one two-electron operator, i.e. $4\pi\delta^3(r_{ab})$, to be regularized. The corresponding \tilde{Q} operators are of the following form: r_a^{-1} , $1/6r_a^{-3}(r_a^i r_a^j - \delta^{ij}r_a^2/3)$ and

r_{ab}^{-1} , respectively.

Another regularization scheme is needed for $\sum_a \vec{p}_a^4$. In this case

$$\sum_a \vec{p}_a^4 = [\sum_a \vec{p}_a^4]_r - 4\{E_0 - H^{(2)}, V\}, \quad (\text{A4})$$

where

$$[\sum_a \vec{p}_a^4]_r = 4(E_0 - V)^2 - 2\sum_{a < b} \vec{p}_a^2 \vec{p}_b^2 - \frac{4}{m_N}(E_0 - V)\vec{p}_N^2 + \frac{1}{m_N^2}\vec{p}_N^4 \quad (\text{A5})$$

Using this definition the following identity can be written

$$\langle \Psi | \sum_a \vec{p}_a^4 | \Psi \rangle = \langle \Psi | [\sum_a \vec{p}_a^4]_r | \Psi \rangle. \quad (\text{A6})$$

Finally, we make use of the following regularization scheme for the Araki-Sucher term (in the infinite mass limit) [29]

$$\begin{aligned} \left\langle \Psi \left| P \left(\frac{1}{r_{ab}^3} \right) \right| \Psi \right\rangle &= \sum_c \left\langle \Psi \left| \vec{p}_c \frac{\ln r_{ab}}{r_{ab}} \vec{p}_c \right| \Psi \right\rangle \\ &+ \left\langle \Psi \left| 4\pi(1 + \gamma)\delta(r_{ab}) + 2(E_0 - V)\frac{\ln r_{ab}}{r_{ab}} \right| \Psi \right\rangle. \end{aligned} \quad (\text{A7})$$

Appendix B: Table of u- coefficients

[1] W. Nörterhäuser, C. Geppert, A. Krieger, K. Pachucki, M. Puchalski, K. Blaum, M. L. Bissell, N. Frömmgen, M. Hammen, M. Kowalska, J. Krämer, K. Kreim, R. Neugart, G. Neyens, R. Sánchez, and D. T. Yordanov, Precision test of many-body QED in the Be^+ $2p$ fine structure doublet using short-lived isotopes, *Phys. Rev. Lett.* **115**, 033002 (2015).

[2] K. Pachucki, V. Patkóš, and V. A. Yerokhin, Testing fundamental interactions on the helium atom, *Phys. Rev. A* **95**, 062510 (2017).

[3] S. Alighanbari, G. S. Giri, F. L. Constantin, V. I. Korobov, and S. Schiller, Precise test of quantum electrodynamics and determination of fundamental constants with HD^+ ions, *Nature* **581**, 152 (2020).

[4] R. Sánchez, W. Nörterhäuser, G. Ewald, D. Albers, J. Behr, P. Bricault, B. A. Bushaw, A. Dax, J. Dilling, M. Dombsky, G. W. F. Drake, S. Götte, R. Kirchner, H.-J. Kluge, T. Kühl, J. Lassen, C. D. P. Levy, M. R. Pearson, E. J. Prime, V. Ryjkov, A. Wojtaszek, Z.-C. Yan, and C. Zimmermann, Nuclear charge radii of ${}^{9,11}\text{Li}$: The influence of halo neutrons, *Phys. Rev. Lett.* **96**, 033002 (2006).

TABLE VII. Matrix elements reduction coefficients, see Sec. IV A.

P_l	$2u_l$ (singlet)	$2u_l$	$2u_l^1$	$2u_l^2$	$2u_l^3$	$2u_l^4$	$2u_l^{12}$	$2u_l^{13}$	$2u_l^{14}$	$2u_l^{23}$	$2u_l^{24}$	$2u_l^{34}$
1234	2	2	0	0	2	2	0	0	0	0	0	-2
1243	2	-2	0	0	-2	-2	0	0	0	0	0	2
1324	-1	-1	1	-1	-1	-1	0	0	-1	0	1	1
1342	-1	1	-1	1	1	1	0	0	1	0	-1	-1
1423	-1	1	-1	1	1	1	0	1	0	-1	0	-1
1432	-1	-1	1	-1	-1	-1	0	-1	0	1	0	1
2134	2	2	0	0	2	2	0	0	0	0	0	-2
2143	2	-2	0	0	-2	-2	0	0	0	0	0	2
2314	-1	-1	-1	1	-1	-1	0	0	1	0	-1	1
2341	-1	1	1	-1	1	1	0	0	-1	0	1	-1
2413	-1	1	1	-1	1	1	0	-1	0	1	0	-1
2431	-1	-1	-1	1	-1	-1	0	1	0	-1	0	1
3124	-1	-1	1	-1	-1	-1	0	0	-1	0	1	1
3142	-1	1	-1	1	1	1	0	0	1	0	-1	-1
3214	-1	-1	-1	1	-1	-1	0	0	1	0	-1	1
3241	-1	1	1	-1	1	1	0	0	-1	0	1	-1
3412	2	0	0	0	0	0	0	1	-1	-1	1	0
3421	2	0	0	0	0	0	0	-1	1	1	-1	0
4123	-1	1	-1	1	1	1	0	1	0	-1	0	-1
4132	-1	-1	1	-1	-1	-1	0	-1	0	1	0	1
4213	-1	1	1	-1	1	1	0	-1	0	1	0	-1
4231	-1	-1	-1	1	-1	-1	0	1	0	-1	0	1
4312	2	0	0	0	0	0	0	1	-1	-1	1	0
4321	2	0	0	0	0	0	0	-1	1	1	-1	0

[5] S. Sturm, F. Köhler, J. Zatorski, A. Wagner, Z. Harman, G. Werth, W. Quint, C. H. Keitel, and K. Blaum, High-precision measurement of the atomic mass of the electron, *Nature* **506**, 467 (2014).

[6] T. Manovitz, R. Shaniv, Y. Shapira, R. Ozeri, and N. Akerman, Precision measurement of atomic isotope shifts using a two-isotope entangled state, *Phys. Rev. Lett.* **123**, 203001 (2019).

[7] B. Maaß, T. Hüther, K. König, J. Krämer, J. Krause, A. Lovato, P. Müller, K. Pachucki, M. Puchalski, R. Roth, R. Sánchez, F. Sommer, R. B. Wiringa, and W. Nörtershäuser, Nuclear charge radii of $^{10,11}\text{B}$, *Phys. Rev. Lett.* **122**, 182501 (2019).

[8] N. J. Stone, Nuclear magnetic dipole and electric quadrupole moments: Their measurement and tabulation as accessible data, *J. Phys. Chem. Ref. Data* **44**, 031215 (2015).

[9] M. Puchalski, J. Komasa, and K. Pachucki, Hyperfine structure of the 2^3P state in ^9Be and the nuclear quadrupole moment, *Phys. Rev. Research* **3**, 013293 (2021).

[10] E. Tiesinga, P. J. Mohr, D. B. Newell, and B. N. Taylor, CODATA recommended values of the fundamental physical constants: 2018, *Rev. Mod. Phys.* (2021), in press.

[11] M. S. Safronova, D. Budker, D. DeMille, D. F. J. Kimball, A. Derevianko, and C. W. Clark, Search for new physics with atoms and molecules, *Rev. Mod. Phys.* **90**, 025008 (2018).

[12] V. A. Yerokhin and K. Pachucki, Theoretical energies of low-lying states of light helium-like ions, *Phys. Rev. A* **81**, 022507 (2010).

[13] V. Patkóš, V. A. Yerokhin, and K. Pachucki, Radiative α^7m QED contribution to the helium Lamb shift, *Phys. Rev. A* **103**, 012803 (2021).

[14] W. Nörtershäuser, D. Tiedemann, M. Žáková, Z. Andjelkovic, K. Blaum, M. L. Bissell, R. Cazan, G. W. F. Drake, C. Geppert, M. Kowalska, J. Krämer, A. Krieger, R. Neugart, R. Sánchez, F. Schmidt-Kaler, Z.-C. Yan, D. T. Yordanov, and C. Zimmermann, Nuclear charge radii of $^{7,9,10}\text{Be}$ and the one-neutron halo nucleus ^{11}Be , *Phys. Rev. Lett.* **102**, 062503 (2009).

[15] A. Krieger, K. Blaum, M. L. Bissell, N. Frömmgen, C. Geppert, M. Hammen, K. Kreim, M. Kowalska, J. Krämer, T. Neff, R. Neugart, G. Neyens, W. Nörtershäuser, C. Novotny, R. Sánchez, and D. T. Yordanov, Nuclear charge radius of ^{12}Be , *Phys. Rev. Lett.* **108**, 142501 (2012).

[16] M. Puchalski and K. Pachucki, Quantum electrodynamics corrections to the $2P$ fine splitting in Li, *Phys. Rev. Lett.* **113**, 073004 (2014).

[17] M. Puchalski and K. Pachucki, Ground state hyperfine splitting in $^{6,7}\text{Li}$ atoms and the nuclear structure, *Phys. Rev. Lett.* **111**, 243001 (2013).

[18] M. Wang, G. Audi, F. G. Kondev, W. Huang, S. Naimi, and X. Xu, The AME2016 atomic mass evaluation (II). Tables, graphs and references, *Chin. Phys. C* **41**, 030003 (2017).

[19] R. C. Brown, S. Wu, J. V. Porto, C. J. Sansonetti, C. E. Simien, S. M. Brewer, J. N. Tan, and J. D. Gillaspy, Quantum interference and light polarization effects in unresolvable atomic lines: Application to a precise measurement of the $^{6,7}\text{Li}$ D_2 lines, *Phys. Rev. A* **87**, 032504 (2013).

[20] R. Li, Y. Wu, Y. Rui, B. Li, Y. Jiang, L. Ma, and H. Wu, Absolute frequency measurement of ^6Li D lines with khz-level uncertainty, *Phys. Rev. Lett.* **124**, 063002 (2020).

[21] G. Büssel, H. Kleindienst, and A. Lüchow, Nonrelativistic energies for the Be atom: Double-linked Hylleraas–CI calculation, *Int. J. Quantum Chem.* **66**, 241 (1998).

[22] F. W. King, D. Quicker, and J. Langer, Compact wave functions for the beryllium isoelectronic series, Li^- to Ne^{6+} : A standard Hylleraas approach, *J. Chem. Phys.* **134**, 124114 (2011).

[23] J. S. Sims and S. A. Hagstrom, Hylleraas-configuration-interaction study of the 1S ground state of neutral beryllium, *Phys. Rev. A* **83**, 032518 (2011).

[24] J. Komasa, W. Cencek, and J. Rychlewski, Explicitly correlated gaussian functions in variational calculations: The ground state of the beryllium atom, *Phys. Rev. A* **52**, 4500 (1995).

[25] J. Komasa and J. Rychlewski, 2^1P state of Be from exponentially correlated Gaussian functions, *Chem. Phys. Lett.* **342**, 185 (2001).

[26] J. Komasa, Dipole and quadrupole polarizabilities and shielding factors of beryllium from exponentially correlated Gaussian functions, *Phys. Rev. A* **65**, 012506 (2001).

[27] J. Komasa, J. Rychlewski, and K. Jankowski, Benchmark energy calculations on Be-like atoms, *Phys. Rev. A* **65**, 042507 (2002).

[28] J. Komasa, Lower bounds to the dynamic dipole polarizability of beryllium, *Chem. Phys. Lett.* **363**, 307 (2002).

[29] K. Pachucki and J. Komasa, Relativistic and qed corrections for the beryllium atom, *Phys. Rev. Lett.* **92**, 213001 (2004).

[30] K. Pachucki and J. Komasa, Excitation energy of ${}^9\text{Be}$, *Phys. Rev. A* **73**, 052502 (2006).

[31] M. Stanke, D. Kedziera, S. Bubin, and L. Adamowicz, Ionization potential of ${}^9\text{Be}$ calculated including nuclear motion and relativistic corrections, *Phys. Rev. A* **75**, 052510 (2007).

[32] M. Stanke, D. Kedziera, S. Bubin, and L. Adamowicz, Lowest excitation energy of ${}^9\text{Be}$, *Phys. Rev. Lett.* **99**, 043001 (2007).

[33] M. Stanke, J. Komasa, S. Bubin, and L. Adamowicz, Five lowest 1S states of the Be atom calculated with a finite-nuclear-mass approach and with relativistic and QED corrections, *Phys. Rev. A* **80**, 022514 (2009).

[34] Chen, C. and Gou, B. C., Hyperfine-structure studies of the $1s^22\text{snp}$ ($n=2, 3$) 3P states for the beryllium isoelectronic sequence, *Eur. Phys. J. D* **54**, 545 (2009).

[35] C. F. Bunge, Configuration interaction benchmark for Be ground state, *Theor. Chem. Acc.* **126**, 139 (2010).

[36] K. L. Sharkey, S. Bubin, and L. Adamowicz, An algorithm for calculating atomic D states with explicitly correlated Gaussian functions, *The Journal of Chemical Physics* **134**, 044120 (2011).

[37] C. Chen, Energies, Fine Structures, and Hyperfine Structures of the $1s^22\text{snp}$ ($n=2-4$) States for the Beryllium Atom, *Journal of Atomic, Molecular & Optical Physics*, 569876 (2012).

[38] S. Bubin and L. Adamowicz, Assessment of the accuracy the experimental energies of the ${}^1\text{P}^o$ $1s^22\text{s}6\text{p}$ and $1s^22\text{s}7\text{p}$ states of ${}^9\text{Be}$ based on variational calculations with explicitly correlated Gaussians, *J. Chem. Phys.* **137**, 104315 (2012).

[39] M. Puchalski, J. Komasa, and K. Pachucki, Testing quantum electrodynamics in the lowest singlet states of the beryllium atom, *Phys. Rev. A* **87**, 030502 (2013).

[40] M. Puchalski, K. Pachucki, and J. Komasa, Isotope shift in a beryllium atom, *Phys. Rev. A* **89**, 012506 (2014).

[41] K. L. Sharkey, S. Bubin, and L. Adamowicz, Singlet-triplet energy splitting between ${}^1\text{D}$ and ${}^3\text{D}$ ($1s^22\text{s}nd$), $n=3, 4, 5$, and 6, Rydberg states of the beryllium atom (${}^9\text{Be}$) calculated with all-electron explicitly correlated Gaussian functions, *Chemical Physics Letters* **616**, 254 (2014).

[42] M. Stanke, S. Bubin, and L. Adamowicz, Lowest ten ${}^1\text{P}$ Rydberg states of beryllium calculated with all-electron explicitly correlated Gaussian functions, *Journal of Physics B: Atomic, Molecular and Optical Physics* **52**, 155002 (2019).

[43] A. Kedzierski, M. Stanke, and L. Adamowicz, Atomic fine-structure calculations performed with a finite-nuclear-mass approach and with all-electron explicitly correlated Gaussian functions, *Chem. Phys. Lett.* **751**, 137476 (2020).

[44] E. C. Cook, A. D. Vira, C. Patterson, E. Livernois, and W. D. Williams, Testing quantum electrodynamics in the lowest singlet state of neutral beryllium-9, *Phys. Rev. Lett.* **121**, 053001 (2018).

[45] I. Hornyák, L. Adamowicz, and S. Bubin, Ground and excited 1S states of the beryllium atom, *Phys. Rev. A* **100**, 032504 (2019).

[46] E. C. Cook, A. D. Vira, and W. D. Williams, Resonant two-photon spectroscopy of the $2s3d$ 1D_2 level of neutral ${}^9\text{Be}$, *Phys. Rev. A* **101**, 042503 (2020).

[47] W. R. Bozman, C. H. Corliss, W. F. Meggers, and R. E. Trees, An Intersystem Transition in the First Spectrum of Beryllium, *J. Res. Natl. Bur. Stand. (U.S.)* **50**, 131 (1953).

[48] A. G. Blachman and A. Lurio, Hyperfine structure of the metastable $(1s^22s2p)^3\text{p}$ states of ${}^4\text{Be}^9$ and the nuclear electric quadrupole moment, *Phys. Rev.* **153**, 164 (1967).

[49] A. Kramida, Yu. Ralchenko, J. Reader, and and NIST ASD Team, NIST Atomic Spectra Database (ver. 5.8), [Online]. Available: <https://physics.nist.gov/asd> [2021, February 19]. National Institute of Standards and Technology, Gaithersburg, MD. (2020).

[50] H. A. Bethe and E. E. Salpeter, *Quantum mechanics of one- and two-electron atoms* (Plenum, New York, 1977).

[51] H. A. Bethe, The electromagnetic shift of energy levels, *Phys. Rev.* **72**, 339 (1947).

[52] H. Araki, Quantum-Electrodynamical Corrections to Energy-Levels of Helium, *Progress of Theoretical Physics* **17**, 619 (1957).

[53] J. Sucher, Energy levels of the two-electron atom to order α^3 ry; ionization energy of helium, *Phys. Rev.* **109**, 1010 (1958).

[54] V. Patkóš, V. A. Yerokhin, and K. Pachucki, Complete quantum electrodynamical α^6m correction to energy levels of light atoms, *Phys. Rev. A* **100**, 042510 (2019).

[55] M. I. Eides, H. Grotch, and V. A. Shelyuto, Theory of light hydrogenlike atoms, *Phys. Rep.* **342**, 63 (2001).

[56] M. Puchalski and K. Pachucki, Fine and hyperfine splitting of the $2P$ state in Li and Be^+ , *Phys. Rev. A* **79**, 032510 (2009).

[57] M. Puchalski, J. Komasa, and K. Pachucki, Relativistic corrections for the ground electronic state of molecular hydrogen, *Phys. Rev. A* **95**, 052506 (2017).

[58] A. Hibbert, Developments in atomic structure calculations, *Rep. Prog. Phys.* **38**, 1217 (1975).

[59] A. M. Frolov and D. M. Wardlaw, Triplet 2^3S states in four-electron Be-like ions: Bound-state properties and hyperfine-structure splitting, *Phys. Rev. A* **79**, 064501 (2009).

[60] X.-W. Zhu and K. T. Chung, Energies, fine structures and oscillator strengths of $1s^22\text{p}^2$ ${}^1\text{S}$, ${}^1\text{D}$ and ${}^3\text{P}_{2,1,0}$ states of Be-like ions, *Physica Scripta* **52**, 654 (1995).

[61] M. Stanke and L. Adamowicz, Finite-nuclear-mass calculations of the leading relativistic corrections for atomic D states with all-electron explicitly correlated Gaussian functions, *Phys. Rev. A* **100**, 042503 (2019).

[62] L. Johansson, The spectrum of the neutral beryllium atom, *Ark. Fys.* **23**, 119 (1962).

[63] K. T. Chung and X.-W. Zhu, Energies, fine structures, and isotope shifts of the $1s^22\text{snl}$ excited states of the beryllium atom, *Phys. Rev. A* **48**, 1944 (1993).

[64] C. Fischer and G. Tachiev, Breit-Pauli energy levels, lifetimes, and transition probabilities for the beryllium-like to neon-like sequences, *Atomic Data and Nuclear Data Tables* **87**, 1 (2004).

[65] M. Puchalski, J. Komasa, P. Czachorowski, and K. Pachucki, Nonadiabatic QED Correction to the Dissociation Energy of the Hydrogen Molecule, *Phys. Rev. Lett.* **122**, 103003 (2019).